

DOI: 10.1002/adem.201100048

Characterization of High-Strain Rate Mechanical Behavior of AZ31 Magnesium Alloy Using 3D Digital Image Correlation**

By Yanli Wang*, Hanbing Xu, Donald L. Erdman, Michael J. Starbuck and Srdjan Simunovic

Characterization of the material mechanical behavior at sub-Hopkinson regime (0.1 to 1000 s^{-1}) is very challenging due to instrumentation limitations and the complexity of data analysis involved in dynamic loading. In this study, AZ31 magnesium alloy sheet specimens are tested using a custom designed servo-hydraulic machine in tension at nominal strain rates up to 1000 s^{-1} . In order to resolve strain measurement artifacts, the specimen displacement is measured using 3D Digital Image correlation instead from actuator motion. The total strain is measured up to $\approx 30\%$, which is far beyond the measurable range of electric resistance strain gages. Stresses are calculated based on the elastic strains in the tab of a standard dog-bone shaped specimen. Using this technique, the stresses measured for strain rates of 100 s^{-1} and lower show little or no noise comparing to load cell signals. When the strain rates are higher than 250 s^{-1} , the noises and oscillations in the stress measurements are significantly decreased from ≈ 250 to 50 MPa . Overall, it is found that there are no significant differences in the elongation, although the material exhibits slight work hardening when the strain rate is increased from 1 to 100 s^{-1} .

Material response under dynamic crash loading is an essential aspect for automobile design to assess vehicle crashworthiness and improve safety performance. However, due to challenges in instrumentation, mechanical property characterization at strain rates of $0.1\text{--}10^3\text{ s}^{-1}$ is not standardized, although these conditions are most relevant to

automobile collision scenarios.^[1–4] First, in order to perform high-speed mechanical tests in this strain rate regime, the testing machine actuator is required to have speed capabilities on the order of several hundred in s^{-1} and necessary dynamic load capacity of several thousand pounds. Second, upon high-speed loading, load cells used for force acquisition exhibit significant ringing and the noise in the signal due to wave propagation, inertia effects, and the frequency response of the transducers.^[1,3,5–8] This often results in a great deal of uncertainty in stress analysis. Third, accurate strain measurements in the gage section become more difficult as strain rate increases. The most common method to estimate strains is based on the changes in actuator displacement, i.e., through the linear variable differential transformer (LVDT). However, LVDT is not accurate at high speed due to their limited frequency response. Further, LVDT measurements consist of displacements of the loading train and deformations of the entire specimen, hence the contributions of the machine/loading train compliance to the outputs.^[3] Another popular technique for direct measurement of strains of using resistance strain gages is successful other than the limitations of localized measurements and limited measurement range. Recent advances in non-contact optical displacement/strain measurement methods are a solution to the challenges encountered by LVDT and strain gages.^[9–12] Digital image correlation (DIC) as one of the successful technique among the

[*] Dr. Y. Wang, Dr. H. Xu, Dr. D. L. Erdman, Dr. M. J. Starbuck, Dr. S. Simunovic
Oak Ridge National Laboratory, Oak Ridge, TN 37831, (USA)
E-mail: wangy3@ornl.gov

[**] Research was sponsored by the US Department of Energy, Assistant Secretary for Energy Efficiency and Renewable Energy, Office of Transportation Technologies, Lightweight Materials Program, under contract DE-AC05-00OR22725 with UT-Battelle, LLC. Setup of the Digital Image System is through collaboration with Correlation Solution, Inc. This research was partially sponsored by the US Department of Energy, Office of Energy Efficiency and Renewable Energy, Vehicle Technologies Program through the Oak Ridge National Laboratory's High Temperature Materials Laboratory User Program. The discussions and advice from Vlastimil Kunc are appreciated. The authors are also grateful for the help with the experiments from student interns: Emmabeth Parish, Emmanuelle Torchon, Michael C. Wilson, Lauren N. Myers, and Niclas A. West.

optical method family is employed in this study because of its capability of providing detailed information about displacement at each point on the sample surface using full field 3D image analysis.^[9,10]

Mechanical behaviors of light weight metals under dynamic loading have attracted more attention due to their potential applications in automotive industries to satisfy the goal of vehicle weight reduction and fuel efficiency improvement, and among which, magnesium alloys are being considered as one of the most promising structural material candidates owing to their high strength-to-weight ratios.^[13–16] In this paper, we report on the development of techniques to generate reliable stress strain curves within the sub-Hopkinson strain rate regime for sheet metal magnesium AZ31 specimens. Stresses are calculated from the elastic strain in the specimen tab region, and the displacement of the tensile specimens was successfully resolved with a DIC 3D high-speed imaging system. Since this technique has a major advantage over the conventional indirect measurement methods, the data analysis has avoided ambiguity and the results are more consistent.

Experimental

High-Rate Servo-Hydraulic Test Machine

The heart of the high-rate test machine (HRTM) consists of a custom high-rate actuator designed and built by MTS. Capacity is 9000 lbs at static conditions and 5500 lbs at maximum velocity of 700 in·s⁻¹. The stroke range is 15.5 inches of travel. The actuator has a single 400 gpm servo-valve supplied by two 5 gallon accumulators, all driven with an MTS 407 servo-hydraulic controller. The actuator is mounted in a recycled MTS 100 kip, two post load frame. Attached to the actuator is a slack adapter which allows it to travel up 7 inches before engaging and loading the specimen. This enables the machine to accelerate up to full speed and engage the specimen at constant velocity. Along with the slack adapter the other components of the load train that are specifically designed for high-rate testing are low mass titanium alloy grips. The objective of reducing the moving mass between the sample the load cell is to increase the Eigen frequency of the test set-up, hence its effect on the stress–strain curves during high strain testing is minimized.^[3]

For most situations, machine transducers include a DC strain gage load cell along with a charge amplified piezoelectric load cell (Kistler) with capacities up to 9000 lbs. Actuator displacement is measured with a MTS Temposonic acoustic transducer due to the high velocities which would be outside the range of LVDT displacement measurements. All of the aforementioned are conditioned through the model 407 controller.

Data Acquisition

Due to the unique requirements of the high-rate testing, multiple data sources are needed for synchronization. Custom

software was developed in-house. All the software is written in LabView and the hardware for the data acquisition (DAQ) and control is primarily National Instruments (NI) products for ease of integration with LabView. The basic operation of the system consists of simultaneous synchronized signal generation and DAQ on a NI multi-purpose M-series board (16 bit A/D, D/A, PXI 6251). The waveform from the control drives the external input to the servo-hydraulic model 407 controller which controls the high-rate actuator. Waveforms consist of linear ramps which result in constant velocities up to the maximum speed. The generated waveform is synchronized through software triggering to high-speed digital image systems. An NI PXI chassis houses all DAQ and control cards and communication to the controlling computer is done through a MXI-3 fiber optic interface. Additional cards are employed in the PXI chassis on an *ad hoc* basis depending on the channel count or specific need for various tests. Synchronization of all the data sources is within approximately 10 μs.

Digital Image System

Three-dimensional Digital Image System is adopted in this study to improve sample design and analyze displacements of the gage section. The system is equipped with two high-speed digital cameras (Photron FASTCAM SA5) which provide 7 500 frames per s (fps) at resolution of 1024 × 1024 pixels and reduced resolution operation to 1000000 fps. These two cameras are staged so that the area of interest on the sample is visible to both cameras. Prior to the tests, a standard calibration procedure is performed to determine the camera parameters such as focal length, radial distortion coefficients, center position of the lens, skew of the sensor grid, and the relationship between the two cameras. A rigid calibration grid with known spacing is used to perform the calibration. Within the depth of field, images are taken simultaneously while the calibration grid is placed to cover the image field and positioned to have tilt/rotation and translation along all three axes. An acceptable calibration for this study is when the standard deviation of residuals for a minimum 20 views of the calibration grid at various positions is less than 0.05 pixels. During the tensile tests, sequential images are simultaneously recorded by both cameras. The images are post-processed to form 3D deformation contours based on a pattern-matching algorithm^[9] using the commercial software VIC-3D 2007 (Correlated Solutions, Inc.). This algorithm uses subset-based normalized cross-correlation criteria by comparing the reference subset in subsequent images. After analysis, Lagrangian strain, ϵ_{Lagr} , or engineering strain, ϵ_{eng} , can be extracted from the area of interest. For uniform deformation, these two types of strain are related through:

$$\epsilon_{eng} = \sqrt{1 + 2(\epsilon_{Lagr})} - 1 \quad (1)$$

where $\epsilon_{eng} = (L - L_0)/L_0$ with L_0 and L defined as the original length and the deformed length of the specimen, respectively.

Materials and Sample Preparation

The tensile specimens are electric-discharge-machined from the as received AZ31 magnesium sheet metal along the rolling direction. The nominal specimen thickness is 1.9 mm. The sample geometry is schematically shown in Figure 1. The 4-in tab end was hooked to the load cells (known as the “fixed end”) and the 2-in tab end was connected to the slack adapter through titanium alloy grips. CEA-06-125UN-350 strain gages (Vishay Micro-Measurements) are attached onto tab section 1.5 inches away from the grip and the gage section to minimize the effect of gripping and ensure uniform elastic deformation during entire loading process. Each specimen is sanded and cleaned before being gauged. All strain gages are mounted with AE15 adhesive and cured for 3 h at 140 F. In addition, strain gages signals are conditioned through Vishay 2310 conditioners with wide-band filter.

The above specimen geometry for the studied material ensures uniform elastic deformation at the strain gage locations on the tab, therefore, the load can be backed out through Hooke’s law:

$$P = E \varepsilon_{eng} A_0 \tag{2}$$

where P is the load, ε_{eng} the engineering strain, E the elastic modulus and a value of 45 GPa was used for magnesium alloy, and A_0 is the cross-section area of the tab.

A random black and white speckle pattern was created on the specimen surface using Rust-Oleum primer and Ceylon ultra flat black spray paints. These patterns provide reference for DIC process. In order to improve adhesion between the spray paint and the specimen surface, a specific surface treatment was performed. For specimens used for test speeds less than $10 \text{ in} \cdot \text{s}^{-1}$, the surfaces were sanded with 400 grit sand paper and cleaned with acetone, whereas those at test speeds higher than $100 \text{ in} \cdot \text{s}^{-1}$ specimens were sandblasted. The paints were applied within 1–2 h prior to the tensile tests as over-drying resulted in delamination of the paint when the test speed was higher than $100 \text{ in} \cdot \text{s}^{-1}$.

Results and Discussions

Digital Image Correlation for Sample Deformation

With the DIC system, a 3D full field deformation map is generated within the area of interested. In this study, information from the full field deformation map was used to assist specimen design and derive the true strain rate. Figure 2 depicts an example of the analysis for a specimen that was loaded at $10 \text{ in} \cdot \text{s}^{-1}$ (strain rate of 10 s^{-1}). The 3D

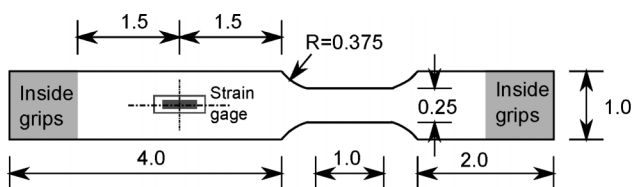


Fig. 1. Schematics of the tensile specimen geometry (dimensions are in inches).

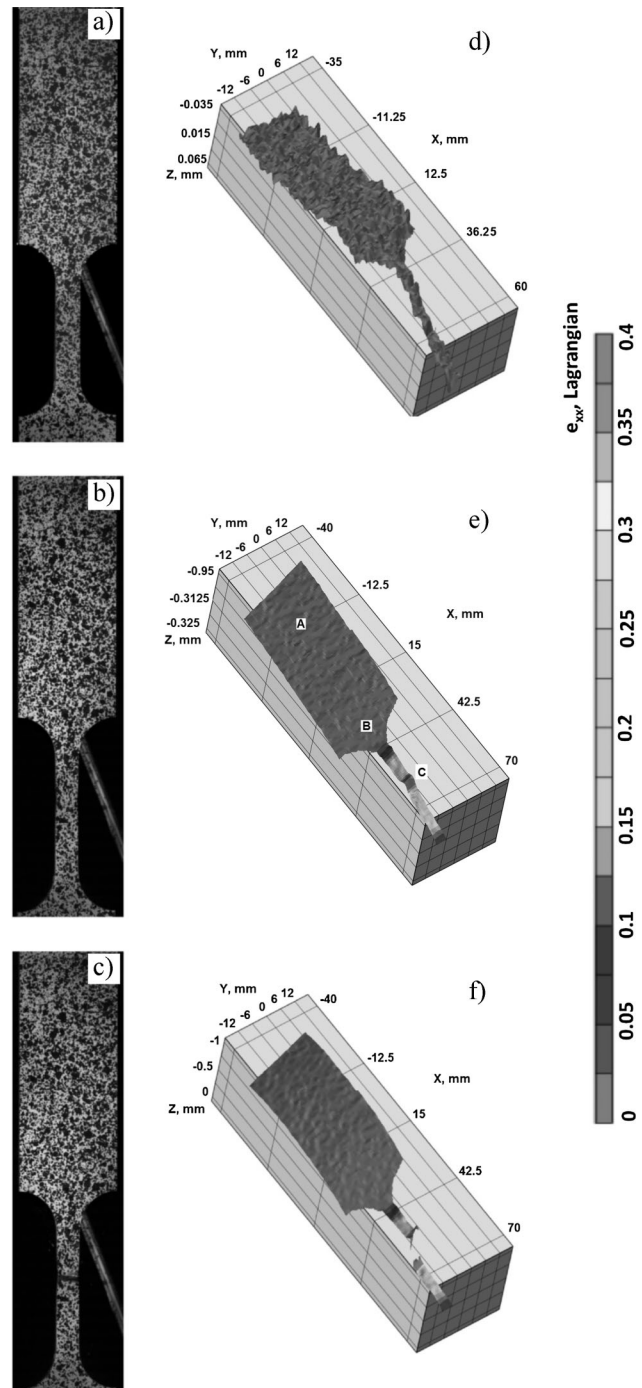


Fig. 2. Digital image correlation analysis with images taken by one of the cameras showing (a) before loading, (b) necking, and (c) post test; the corresponding post analysis (d), (e), and (f) show the full field Lagrangian strain fields. The highlighted region in (a) is the area of interest.

Lagrangian strain plots are the results of DIC post analysis on the area of interested selected from the original image pairs taken by the high-speed cameras.

Prior to loading, the specimen was found not to be perfectly flat [shown in Fig. 2(d)], evidently shown from the 3D DIC post analysis. The warpage of the samples within the 1 in gage section is approximately 0.1 mm. This sample condition may

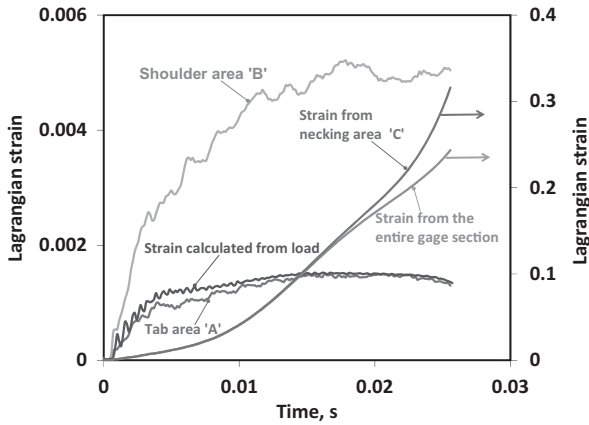


Fig. 3. Comparison of the Lagrangian strains on the specimen.

be due to the combination of cold rolling process for the as-received sheet and EDM machining. Before the sample failed, the specimen exhibited significant necking behavior (the red region inside the gage in Fig. 2e). The load train in this study is not perfectly stiff and there is some slack between the extension bars and the slack adapter and clevis attachments, hence the sample tends to experience some out-of-plane motion, i.e., rotation around loading direction (X-direction) and slightly shift position along Z-direction, as evidenced in images Figure 2(d)–(f). It needs to be pointed out that, 3D Digital Image Correlation (DIC) system processed the images and minimized error caused by out-of-plane motions in deformation measurement,^[10] and therefore the imperfections in the test setup do not affect the accuracy of the strain measurements.

From the full field Lagrangian strain map, the local strains at various positions on the sample were extracted and compared in Figure 3. On the tab where the strain gage (see Fig. 1 and location “A” in Fig. 2) is located, the maximum strain was measured to be 0.0015. This strain level confirms that the tab was under elastic deformation during the entire loading process. The strain at location ‘A’ matches well with the average tab strains backed out from load cell signal using Equations 1 and 2. This sample geometry with tab width to gage width ratio to be four guarantees the tab only deforms elastically and the elastic strain in the tab is significant enough to be resolved accurately through strain gages or DIC. In addition, the slight differences between these two strains are due to instantaneous bending of the specimen during loading

because of the compliance in the load train. Similar observations of instantaneous bending behavior under high-strain rate were made by other studies.^[1,3] It is concluded that in order to obtain load values from elastic strains in the tab, the average values of both tab surfaces should be used. The comparison between the strains extracted from the necking region “C” and the average strains from the entire gage section indicates that the specimen deformed uniformly to $\approx 13\%$ and then deform locally at location “C”. The average strain rate for this test calculated from the uniform plastic deformation region is 9.7 s^{-1} and close to the nominal strain rate of 10 s^{-1} .

Strain Rate Effect

In order to assess strain rate effect on material mechanical behavior, one has to start with accurate measurement of strains or displacements as a function of time. This is especially true for strain rate sensitive materials. At high-strain rates, the LVDT cannot resolve strain with enough accuracy. In this study, the accurate strain rate is calculated from the uniform plastic deformation region (between yield and the maximum tensile strength) in the gage section acquired by DIC system, i.e., from yielding to strain of $\approx 14\%$. Table 1 summarized the nominal strain rates (the command signal in the DAQ software), strain rates which was calculated from LVDT signals and the accurate strain rates which was measured at the gage section using DIC for all the tests performed in this study. It shows that at strain rates of 1 and 10 s^{-1} , LVDT signal and DIC signal matches the nominal strain rates. However, it shows quite large deviations when the nominal strain rate is higher than 100 s^{-1} . The LVDT showed quite large differences compared to DIC. For example, at nominal strain rate of 250 s^{-1} , the strain rate was measured to be $\approx 295\text{ s}^{-1}$ by LVDT, but actually it was 547 s^{-1} . The difference between LVDT and actual strain rate does not show linear relationship with nominal strain rate. Therefore, it is suggested by this study that one has to use proper techniques to measure the deformations in the gage section to resolve strain rate when using similar hydraulic testing set-ups to evaluate strain rate effects on material mechanical behaviors.

At strain rates of 1 and 10 s^{-1} , the stress can be evaluated from load washer or backed out from the elastic strain on the tab. However, it is challenging to resolve the stresses when the loading rate is higher than 10 s^{-1} due to the noises and ringing in the load washer. Figure 4 shows an example of the specimen

Table 1. Summary of the high-strain rate tensile results for AZ31.

Nominal strain rate [s^{-1}]	Number of samples tested	Strain rate from LVDT [s^{-1}]	Strain rate from DIC [s^{-1}]	UTS, [MPa]	Total elongation Lagrangian strain
1	3	1	0.9	291 ± 11	0.22 ± 0.01
10	2	8.2, 10.1	10.5, 9.7	302, 295	0.24, 0.24
100	4	90 ± 4	71 ± 3	310 ± 3	0.19 ± 0.04
250	2	295, 403	547, 565	338, 331	0.23, 0.19
500	3	437 ± 92	856 ± 118	344 ± 6.6	0.27 ± 0.02
1000	4	867 ± 105	$1\ 183 \pm 52$	356 ± 10.7	0.27 ± 0.04

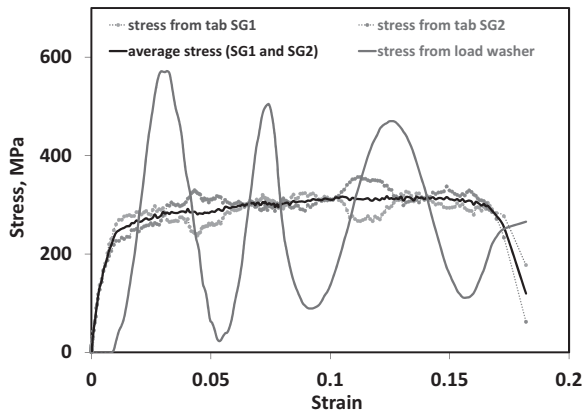


Fig. 4. Stress strain curve of AZ31 at 71 s^{-1} .

loaded at strain rate of 71 s^{-1} , ringing in the load washer signal is so significant that generation of a meaningful stress strain curve is difficult without taking into account the effects of mechanical wave propagation. In order to solve this problem, the stresses were calculated from the strain gage signals on the tab. After yielding, it is found that the strain signals on the two opposite tab surfaces showed anti-phase characteristics, indicating the two opposite surfaces experienced vibration in the opposite directions. This observation is consistent with instantaneous bending phenomena that often found in high-strain rate test due to the non-perfect stiff load train.^[3] When the average values from the strain gages on the two tab surfaces are used to calculate the stress, the results are found to be in line with intrinsic material behavior.

In order to characterize strain effect on AZ31 alloy, specimens were tested at nominal strain rates of 1, 10, 100, 250, and 500 s^{-1} with 1 in gage length, respectively. A half inch gage length specimen was tested at $500 \text{ in} \cdot \text{s}^{-1}$ to reach nominal 1000 s^{-1} strain rate. At least two tests were performed under each condition. The results are also summarized in Table 1. The comparison of the stress strain curves are shown in Figure 5. When the nominal strain rate is 250 s^{-1} and higher, the stress strain curves show some level of oscillatory behavior, the ultimate tensile strength (UTS) is

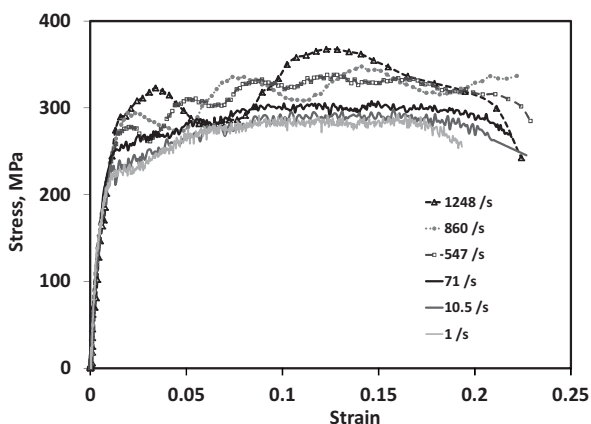


Fig. 5. Strain rate effect on AZ31 magnesium alloy.

simply taken as the highest stress level. Although it shows some level of oscillatory behavior, the noises and oscillations in the stress measurements were significantly decreased from ≈ 250 to 50 MPa when it is compared to the load cell signals. This oscillation in the stress strain curves is suspected to be associated with the characteristics of the sample itself and the loading train.

To summarize the strain rate effect, no significant difference in the elongation was observed for AZ31 when strain rate increases from 1 to 1000 s^{-1} , although the material exhibited slight work hardening and small strain rate sensitivity within the testing region. This observation is consistent with literature reported mechanical behavior of AZ31 alloy under quasi-static loading condition^[17] and the twinning deformation mechanisms for magnesium alloys.^[18]

Conclusions

Three-dimensional DIC technique was successfully applied to high speed tests at up to 1000 s^{-1} . Post analysis using DIC can resolve true sample deformation without being affected by the out-of-plane motion. It is also found that when average elastic strains from the opposite specimen tab surfaces are used to back out stresses, the stress strain curves show intrinsic material behavior. For strain rate sensitive materials tests at the studied strain rate range, strains must be accurately measured inside the gage section rather than using LVDT signals. When strain rate increases from 1 to 1000 s^{-1} , AZ31 exhibited slight work hardening without noticeable sacrifice of elongation.

Received: March 16, 2011

Published online: May 17, 2011

- [1] J. H. Lim, *POSCO Tech. Report* **2007**, 10, 116.
- [2] A. Rusinek, R. Cheriguene, A. Bäumer, J. R. Klepaczko, P. Larour, *J. Strain Anal.* **2008**, 43, 37.
- [3] P. Larour, J. Noack, W. Bleck, *MP Mater. Testing* **2009**, 51, 184.
- [4] R. Othman, P. Guégan, G. Challita, F. Pasco, D. Lebreton, *Int. J. Impact Eng.* **2009**, 36, 460.
- [5] P. K. C. Wood, C. A. Schley, in: *Strain Rate Testing of Metallic Materials and Their Modelling for use in CAE based Automotive Crash Simulation Tools (Recommendations and Procedures)*, Smithers, UK **2009**, Ch. 6.
- [6] H.-S. Shin, H.-M. Lee, M.-S. Kim, *Int. J. Impact Eng.* **2000**, 24, 571.
- [7] B. L. Boyce, T. B. Crenshaw, *Sandia Report* **2005**, SAN D2005-5678, DOI: 10.2172/875626.
- [8] Ph. Béguelin, M. Barbezat, H. H. Kausch, *J. Phys. III France* **1991**, 1, 1867.

- [9] M. A. Sutton, J.-J. Orteu, H. W. Schreier, in: *Image Correlation for Shape Motion and Deformation Measurements*, Springer, USA **2009**, Ch. 5, 9.
- [10] M. A. Sutton, J. H. Yan, V. Tiwari, H. W. Schreier, J.-J. Orteu, *Opt. Lasers Eng.* **2008**, *46*, 746.
- [11] J. D. Helm, *Exp. Mech.* **2008**, *48*, 753.
- [12] G. Huang, H. Zhu, B. Yan, *SAE Int.* **2009**, 2009-01-0470, DOI: 10.4271/2009-01-0470.
- [13] B. L. Mordike, T. Ebert, *Mater. Sci. Eng. A* **2001**, *A302*, 37.
- [14] M. Hakamadaa, T. Furutaa, Y. Chinob, Y. Chena, H. Kusudaa, M. Mabuchia, *Energy* **2007**, *32*, 1352.
- [15] F. Pan, M. Bao, J. Wang, J. Peng, A. Tang, *Trans. Non-ferrous Met. Soc. China* **2008**, *18*, s1.
- [16] A. Yamashita, Z. Horita, T. G. Langdon, *Mater. Sci. Eng.* **2001**, *A300*, 142.
- [17] M. Marya, L. G. Hector, R. Verma, W. Tong, *Mater. Sci. Eng.* **2006**, *A418*, 341.
- [18] M. R. Barnett, N. Stanford, P. Cizek, A. Beer, Z. Xuebin, Z. Keshavarz, *JOM* **2009**, *61*, 19.
-